CORROSION SCIENCE AND TECHNOLOGY, Vol.31, No.4(2002), pp.299~305

Stress Corrosion Cracking of Annealed Carbon Steel in Aqueous Bicarbonate Solution

Takumi Haruna, Liehong Zhu, Makoto Murakami, and Toshio Shibata

Department of Materials Science and Processing, Graduate School of Engineering, Osaka University
2-1 Yamada-oka, Suita, Osaka, 565-0871, JAPAN

Effects of potential and concentration of bicarbonate on stress corrosion cracking (SCC) of annealed SM400B carbon steel has been investigated in bicarbonate solutions at 343 K. A potentiostatic slow strain rate testing apparatus equipped with a charge coupled device camera system was employed to evaluate SCC susceptibility from the viewpoint of the crack initiation as well as propagation. Surface of the specimen annealed at more than 1073 K for 3.6 ks had decarburized layer of about 500 μm thickness, and suffered SCC in bicarbonate solutions. In 1 M bicarbonate solution, a lot of cracks were observed in the potential range from -800 to 600 $mV_{Ag/AgCl}$. In the range, both initiation and propagation of the cracks were most accelerated at -600$mV_{Ag/AgCl}$. While, under a constant applied potential of -600mV, many cracks were observed in the concentration range from 0.001 to 1 M, and both initiation and propagation of the cracks were suppressed as the concentration decreased. Polarization curves for the decarburized specimen were measured by two different scan rates. The potential showing larger difference between the current densities measured at the two scan rates predicts that of high susceptibility of SCC initiation. It was found that the potential where large difference between the current densities was -600$mV_{Ag/AgCl}$ for 1M bicarbonate solution, and increased with decrease in the concentration. This suggests that the applied potential of -600$mV_{Ag/AgCl}$ provides high SCC susceptibility for 1M bicarbonate solution, and decrease in the concentration reduces the SCC susceptibility at -600$mV_{Ag/AgCl}$. These predictions was in good agreement with the empirical SCC results depending on the potential as well as the concentration.

Keywords : *stress corrosion cracking, SM400B carbon steel, sodium bicarbonate, anneal, crack initiation, crack propagation, decarburization*

1. Introduction

Some countries possessing nuclear power plants have been discussing the methods to dispose high level radioactive wastes produced by nuclear power generation. A candidate method is so-called 'geological disposal' method, in which the high level radioactive wastes are packed with glass, overpack material and compacted bentonite, and then disposed in underground of about 1000 m depth. In this method, an overpack may be required to remain intact for more than 1000 years to provide containment of radionuclides. Carbon steel is one of the candidate materials for the overpack in Japan.[1] Since carbon steel is easy to occur general corrosion (difficult to occur localized corrosion), corrosion allowance of the carbon steel overpack can be estimated accurately for ensuring its life time. However, there exist some studies on localized corrosion of carbon steels in underground environments, so that further extended works are required to decide selection of carbon steel for the overpack material.[2] Kowaka and Kitamura studied the effect of annealing condition on stress corrosion cracking (SCC) behavior of carbon steel in boiled alkali solution, and revealed that SCC is inhibited under (ferrite + pearlite) structure, and accelerated under austenite structure.[3] This may suggest the heating condition of welding, etc. to carbon steel induces SCC even in weak alkali solutions which may be simulated underground water.[4] Therefore, we have investigated SCC behavior of annealed carbon steel in bicarbonate solutions by using slow strain rate technique from viewpoint of crack initiation and propagation.

2. Experimental

SM400B carbon steel (C:0.12, Si:0.15, Mn:0.64, P:0.002, S:0.004 in mass%) sheet was machined out to plate type smooth tensile specimens having the gauge section of 20 mm^L x 4 mm^W x 2 mmt. The specimen was annealed at 973 to 1223 K for 3.6 ks in Ar flow, followed by cooling at 100 K/3.6 ks. The specimen was mechanically polished

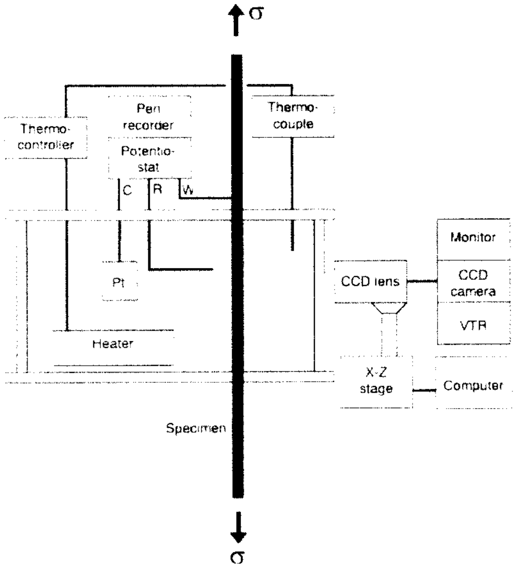

Fig. 1. Schematic illustration of a slow strain rate testing apparatus with dynamic observation system.

up to #3/0 to remove the oxide layer of about 100 μm, and then employed for an SCC test. Test solutions were $NaHCO_3$ solutions at 0.001 to 1 M controlled by reagent grade chemical and distilled water. Test temperature was 343 K.

A slow strain rate testing (SSRT) apparatus with direct observation system shown in Fig. 1 was employed as an SCC test.[5] The system has a unique point of equipping with high performance charge coupled device (CCD) camera system in order to in-situ observe the growth of multiple cracks on the specimen surface during the SCC test. This CCD camera system has long working distance (50 mm in air) as well as long focus depth (about 1 mm in air) in using a lens of 50X in 14" monitor, so that very clear images of crack growth can be obtained through the test solution without re-focussing during the SCC test. In addition, a head part of the CCD camera is mounted on an X-Z stage controlled by a personal computer, and thus multiple cracks over the gauge section can be observed and recorded every 6 hours. An initial strain rate was 8.3×10^{-7} s^{-1}.

Experimental procedure is described here. The polished specimen was mounted to the SSRT cell, and the test solution at room temperature was poured in it. The solution deaerated by N_2 gas for more than 3.6 ks was heated up to 343 K. After the corrosion potential became stable, the given potential from -800 to 600 $mV_{Ag/AgCl}$ was applied to the specimen, and then SSRT started. The potential hereafter is expressed against an Ag/AgCl(3.3 M KCl, RT) reference electrode.

3. Results

3.1 Effect of annealing temperature

The SCC test was conducted for the specimen annealed at 973 to 1223 K for 3.6 ks. The test conditions were 1 M $NaHCO_3$ and -600 mV. It was found that the yield stress and the maximum stress diminished and the fracture strain increased as the annealing temperature increased. The observation of the fractured specimen gave the evidence of intergranular attacks on the specimen annealed at more than 1073 K, as shown in Fig. 2. Whereas, no grain boundary attack appeared on the specimen annealed at more than 1073 K under the same test conditions without stressing, so that the attacks was confirmed to be due to SCC.

Through the direct observation of the specimen surface during the SCC test by the CCD camera system, initiation and propagation behavior of multiple cracks can be grasped in detail. Fig. 3(a) shows the effect of annealing temperature on the time when the first crack is observed (denoted as 'crack initiation time'). As can be seen, the

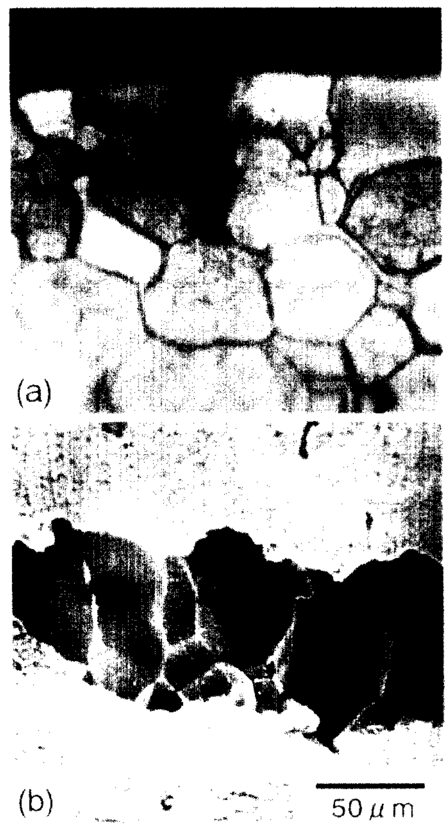

Fig. 2. Appearance of a crack on SM400B steel annealed at 1173 K for 3.6 ks in 1 M $NaHCO_3$ solution under -600 mV. (a)cross sectional view and (b)view from the side surface.

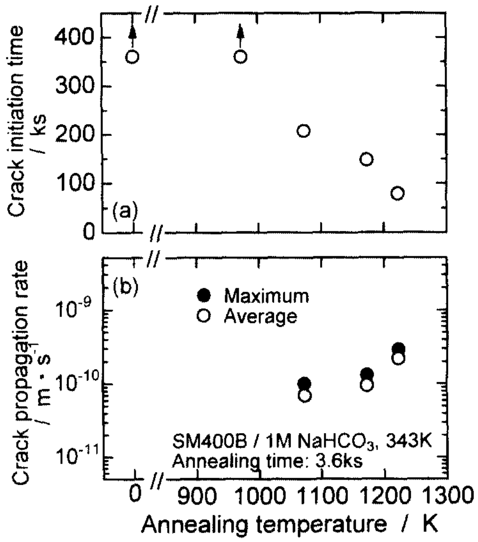

Fig. 3. Effect of annealing temperature on (a)crack initiation time and (b)crack propagation rate for SM400B carbon steel in 1M $NaHCO_3$ at -600 mV.

cracks were initiated at more than 1073 K, and the crack initiation time decreased with increase in the annealing temperature. While, the effect of the annealing temperature on crack propagation rate is shown in Fig.3(b). The crack propagation rate was calculated as follows: Since the individual crack could not be distinguished because of their dense population and small length of about 100 μm at the fracture, so that the depths of some cracks were measured from the cross section of the fractured specimen. Two kinds of crack depth were divided by the time which is the fracture time minus crack initiation time in order to determine a maximum and an average crack propagation rates. The crack propagation rate showed the order of 10^{-10} m s^{-1} (corresponding to order of 1 mm y^{-1}), and increased with increase in the annealing temperature. Therefore, it can be concluded that increase in annealing temperature of more than 1073 K enhances SCC susceptibility by accelerating crack initiation process as well as crack propagation process.

In order to discuss that the SCC appeared at annealing temperature beyond 1073 K, change in microstructure of the material with the annealing temperature was investigated. The results are shown in Fig. 4. The left-hand side edge is the material surface. It is obvious that the microstructure at 973 K is homogeneous structure of ferrite and pearlite, almost same as that of as-received. At more than 1073 K, however, there clearly existed no pearlite phase near the surface, although pearlite band appeared inside the material. The ferrite layer without pearlite thickened as the annealing temperature increased. For example, the layer was about 500 μm at 1173 K for 3.6 ks. Furthermore, the layer thickness is revealed to depend on annealing time.[6] The unique microstructure is quite similar to that of a decarburized steel.[7),8)] While, no such a layer was observed at the surface of the specimen which was packed by silica tube under a vacuum condition of about 10^{-5} Torr and was annealed at 1173 K for 3.6 ks. The furnace, in which Ar gas was flowed during annealing the specimen, is not a completely closed system. Accordingly, some amount of air had to leak into the furnace, and then the slightly oxidized atmosphere had to make the surface layer be decarburized.[8)] The finding strongly suggests that carbon steel should be carefully welded not to form the decarburized layer because of avoiding SCC in relatively concentrated bicarbonate environments.

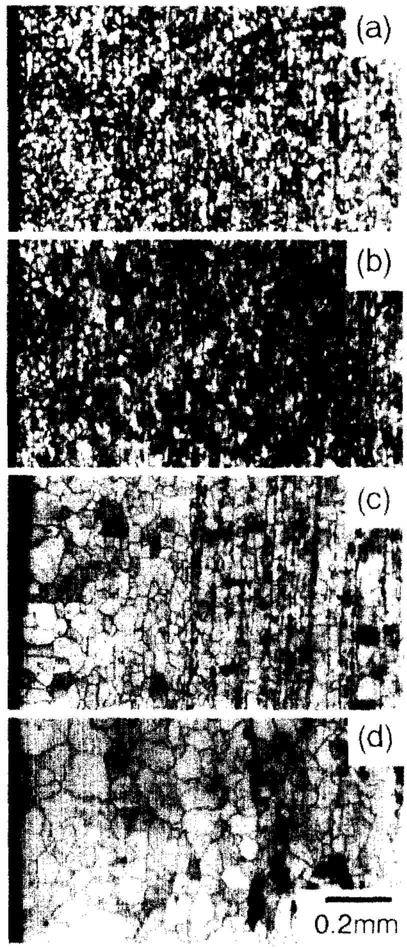

Fig. 4. Change in microstructure of SM400B carbon steel with annealing temperature. (a)as-received, (b)973, (c)1173, and (d)1223 K

3.2 Effect of potential

The SCC test in 1 M $NaHCO_3$ solution at 343 K was carried out for the specimen annealed at 1173 K for 3.6 ks, which had the decarburized layer at the surface region.

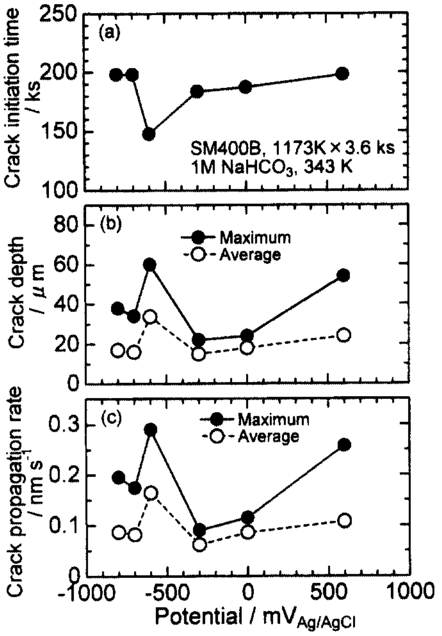

Fig. 5. Effect of applied potential on (a)crack initiation time, (b)crack depth and (c)crack propagation rate for annealed SM400B carbon steel in 1 M $NaHCO_3$ solution.

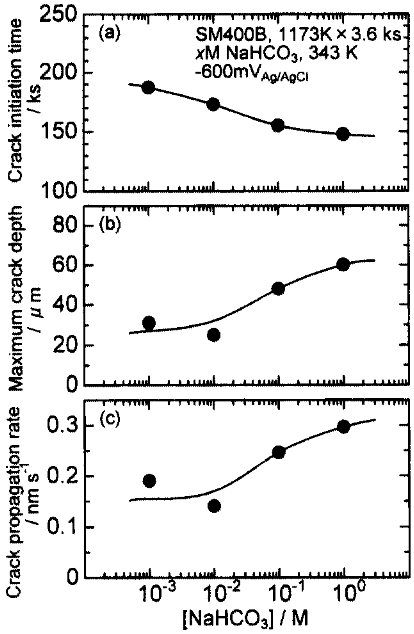

Fig. 6. Effect of concentration of $NaHCO_3$ on (a)crack initiation time, (b)maximum crack depth and (c)maximum crack propagation rate for annealed SM400B carbon steel in $NaHCO_3$ solutions.

There was no remarkable difference in stress-strain curve when the applied potential was changed from -800 to 600 mV. Steady state current density during the SCC test was almost same cathodic value at less than -600 mV, and slightly anodic value at more than -300 mV. SEM observation of surface morphology for the fractured specimen provided a lot of fine cracks over the potential range from -800 to 600 mV.[9)]

Fig. 5 shows the effect of applied potential on crack initiation time, crack depth, and crack propagation rate. As can be seen in these figure, the crack initiation time showed a minimum value at -600 mV, which means that the potential enhances crack initiation process. In addition, crack length and crack propagation rate indicated maximum values at the same potential of -600 mV, which means that the potential also accelerates crack propagation process.

3.3 Effect of bicarbonate concentration

The SCC test for the specimen annealed at 1173 K for 3.6 ks was carried out in $NaHCO_3$ solutions of several concentrations from 0.001 to 1 M. Applied potential was fixed at -600 mV. Shapes of stress-strain curve and current density-strain curve were independent of the concentration of $NaHCO_3$.[9)] However, lots of cracks were observed at the surface of the fractured specimen by SEM.

Fig. 6 shows the effects of crack initiation time, maximum crack depth, and maximum crack propagation rate. The figures clearly demonstrates the following: The crack initiation time increased with decrease in the concentration of $NaHCO_3$, which means that lower concentration of $NaHCO_3$ suppresses crack initiation process. While, maximum crack length and maximum crack propagation rate decreased with decrease in the concentration of $NaHCO_3$, which means that lower concentration of $NaHCO_3$ also suppresses crack propagation process.

4. Discussion

Staehle has considered that SCC is easy to generate under unstable condition of passive films on materials, and proposed three potential regions of SCC generation, which are free corrosion potential, active/passive transition, and passive/transpassive transition regions.[10)] The potential regions have been in good agreement with a lot of SCC systems. Besides, Parkins have developed the electrochemical method to predict SCC generation potential.[11)] This basic concept has quite commonality with that by Staehle. The method is to measure two polarization curves at two different potential scan rates. The polarization curve at higher scan rate provides the electrochemical information on the bare metal surface, which may simulates that at crack tip. On the other hand, the polarization curve at lower scan rate provides the electrochemical information on the surface where some stable film may be formed.

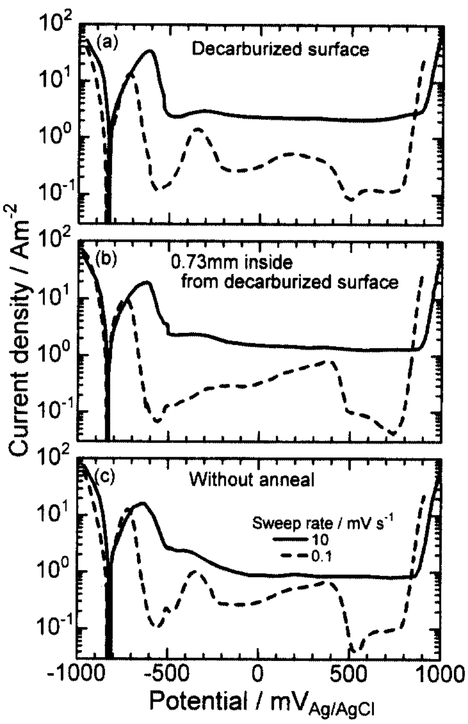

Fig. 7. Polarization curves measured at two scan rate for (a)decarburized surface, (b)the surface 0.73 mm inside from decarburized layer, and (c)the surface of non-annealed SM400B carbon steel in 1 M $NaHCO_3$ solution.

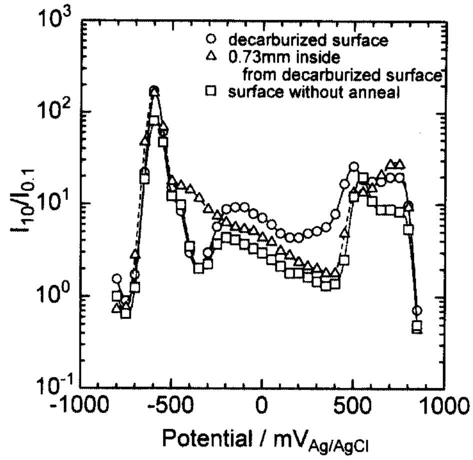

Fig. 8. Ratio of current densities measured at two scan rates plotted against potential from Fig. 7.

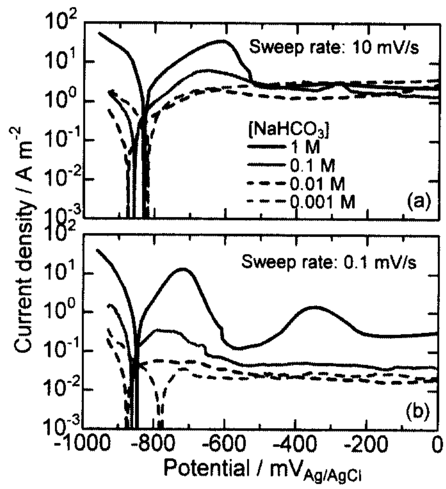

Fig. 9. Polarization curves measured at two scan rate for decarburized SM400B carbon steel in $NaHCO_3$ solution as a function of concentration of $NaHCO_3$.

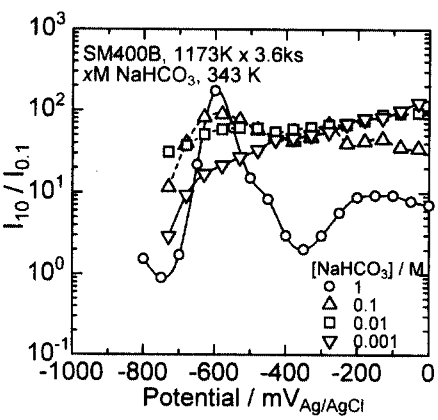

Fig. 10. Ratio of current densities measured at two scan rates plotted against potential from Fig. 9.

The following can be considered at the potential showing large difference between the current densities from the two polarization curves. In the case that the passive film breaks down at the potential, repassivation process at the breakdown site takes place very slowly, namely, the new passive film is unstable, and therefore SCC initiation prefer to occur at the potential. The method has been successfully applied to some SCC systems.[12),13)] Accordingly, the method was applied to the SCC system of this work.

Fig. 7 shows the polarization curves at scan rates of 10 and 0.1 mVs^{-1} in 1 M $NaHCO_3$ solution for the specimen annealed at 1173 K for 3.6 ks. Since the surface morphology was important to the SCC results, three kind of specimen surfaces were prepared: decarburized surface, surface of ferrite and pearlite structure by removing 0.73 mm from the decarburized layer, and non-annealed specimen surface (ferrite and pearlite structure). It is obvious that larger current density is found at higher scan rate under all surface conditions. In addition, active peak current density at higher scan rate is maximum for the decarburized surface.

Ratio of the current densities at the two scan rates ($I_{10}/I_{0.1}$) from the two polarization curves was plotted against the potential, as shown in Fig. 8. It is quite clear that $I_{10}/I_{0.1}$ has a peak at -600 mV for all the surface condition. Therefore, this potential suggests that it is easy to initiate the cracks from the reason mentioned above. In addition, the active peak current density was maximum for the decarburized surface, which corresponds to high crack propagation rate. It is concluded that the decarburized surface is very easy to occur the SCC initiation as well as propagation at -600 mV. The prediction was in good agreement with the SCC result in Fig. 5.

Polarization curves at the two scan rates in $NaHCO_3$ solutions were measured for decarburized specimen annealed at 1173 K for 3.6 ks, as a function of concentration of $NaHCO_3$. The results are shown in Fig. 9. Similar to Fig. 7, current density at higher scan rate is much higher value at all the concentrations. In addition, the current density decreased with decrease in the concentration of bicarbonate.

Fig. 10 shows the ratio of the current densities at the two scan rates ($I_{10}/I_{0.1}$) plotted against the potential as a function of concentration of $NaHCO_3$. In the case of 1 M $NaHCO_3$, there was a peak at -600 mV. However, the peak potential shifted to higher direction as $NaHCO_3$ concentration decreased. As mentioned above, the peak potential predicts high susceptibility of SCC initiation. Fig. 6 demonstrated that SCC susceptibility decreases with decrease in the $NaHCO_3$ concentration. In this study, the constant potential of -600 mV was applied to the specimen during the SCC test. The applied potential coincides to the peak potential in Fig.10 at 1 M $NaHCO_3$, and then the susceptibility of SCC initiation becomes high at this concentration. However, at the lower concentration, the applied potential is far away from the peak potential in Fig.10. Therefore, it is considered that SCC initiation is suppressed at lower concentration. On the other hand, active peak current density of the polarization curves was found to decrease with decrease in the concentration in Fig. 9. This also supports lower crack propagation rate at lower concentration of bicarbonate.

5. Conclusions

1) SM400B carbon steel annealed at more than 1073 K for 3.6 ks in Ar flow containing a small amount of air has decarburized surface layer. The steel with decarburized surface layer suffers SCC in relatively concentrated bicarbonate solutions.

2) The SCC test was carried out in 1 M bicarbonate solution for the steel with decarburized layer by annealing as a function of applied potential, and it was found that the applied potential of -600 $mV_{Ag/AgCl}$ most enhanced crack initiation as well as propagation.

3) The SCC test at applied potential of -600 $mV_{Ag/AgCl}$ was carried out for the steel with decarburized layer by annealing as a function of bicarbonate concentration, and it was found that decrease in the concentration of bicarbonate suppressed crack initiation as well as propagation.

4) Ratio of current densities at two different potential scan rate and active peak current density successfully predicts susceptibility of SCC initiation and propagation, respectively.

References

1. H. Ishikawa, A. Honda, K. Tsurudome, M. Obata, and N. Sasaki, PNC TN8410 92-139, Power Reactor and Nuclear Fuel Development Corporation (1992).
2. T. Haruna, L. Zhu, and T. Shibata, *Corros. Eng.*, **47**, 771 (1998)
3. M. Kowaka and M. Kitamura, *J. Japan Institute of Metals*, **39**, 381 (1975).
4. G. P. Marsh, *Nuclear Energy*, **21**, 253 (1982).
5. T. Shibata and T. Haruna, *Corros. Eng.*, **41**, 809 (1992).
6. T. Haruna, L. Zhu, and T. Shibata, *Corros. Eng.*, **49**, 138 (2000).
7. T. Mochida, *J. Japan Institute of Metals*, **6**, 171 (1942).
8. M. Ochiai, H. Ohba, Y. Tobita, and M. Nagumo, *Tetsu-to-Hagane*, **70**, 2009 (1984).
9. T. Haruna, L. Zhu, M. Murakami, and T. Shibata, *Corros. Eng.*, **49**, 144 (2000).
10. R. W. Steahle, The Theory of Stress Corrosion Cracking, p.223 (1971).
11. R. N. Parkins, *Corros. Sci.*, **20**, 147 (1980)
12. R. N. Parkins, Stress Corrosion Cracking and Hydrogen Embrittlement of Iron Base Alloys, eds. by R. W. Staehle, J. Hochmann, J. E. Slater, and D. McCright, NACE, p.601 (1978).
13. R. N. Parkins and S. Zhou, *Corros. Sci.*, **39**, 175 (1997).